Supportting Information

Room-Temperature Developed Flexible Biomemristor with Ultralow Switching Voltage for Array Learning

Tian-Yu Wang[1†], Jia-Lin Meng[1†], Zhen-Yu He[1], Lin Chen[1]*, Hao Zhu[1], Qing-Qing Sun[1]*, Shi-Jin Ding[1], Peng Zhou[1], and David Wei Zhang[1]

[1]State Key Laboratory of ASIC and System, School of Microelectronics, Fudan University, Shanghai 200433, China

[†]T-Y.W. and J-L.M. contributed equally to this work.

*Correspondence and requests for materials should be addressed to L.C. and Q.Q.S. (E-mail : linchen@fudan.edu.cn; qqsun@fudan.edu.cn;)

S1. The fabrication process of room- temperature developed flexible memristor.

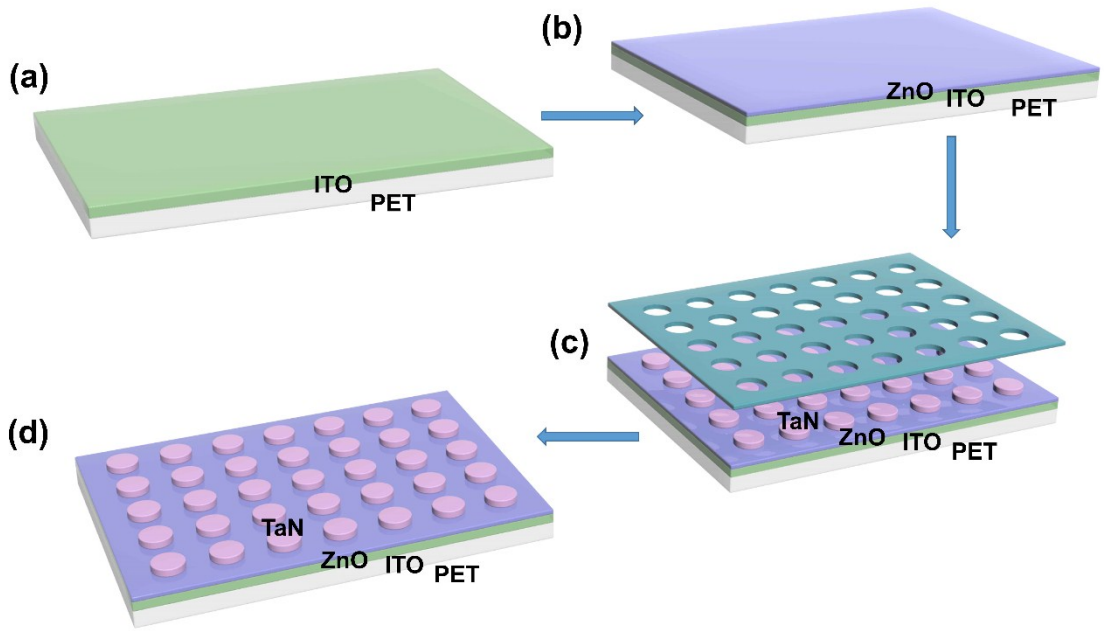

Figure S1. The fabrication flow of device. (a) The substrate of PET/ITO was cleaned and used as flexible substrate, in which the ITO acts as the bottom electrode. (b) The film of ZnO with thickness of ~40 nm was deposited on the flexible substrate by PVD under room temperature. (c) Top electrode of TaN was deposited by PVD using a shadow mask. (d) The low- cost memristor was formed with the structure of PET/ITO/ZnO/TaN.

S2. EDX mapping image of ZnO film on silicon substrate.

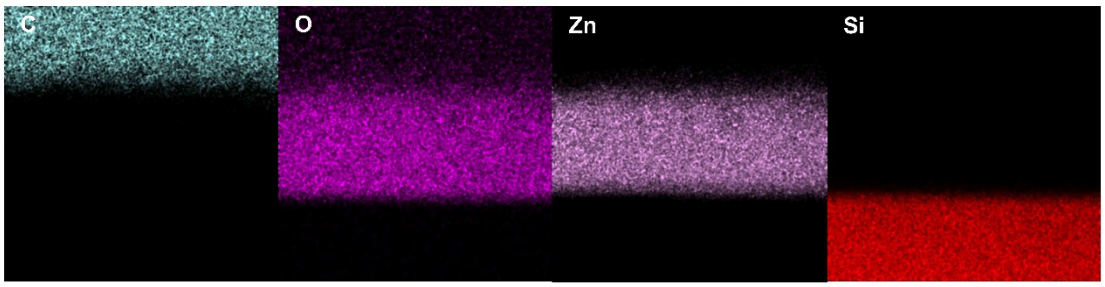

Figure S2. The EDX elemental mapping image of the ZnO film, including C, O, Zn and Si. Note: The film is deposited on the silicon substrate to simplify the EDX mapping test.

S3. The high- resolution XPS spectra of Zn 2p.

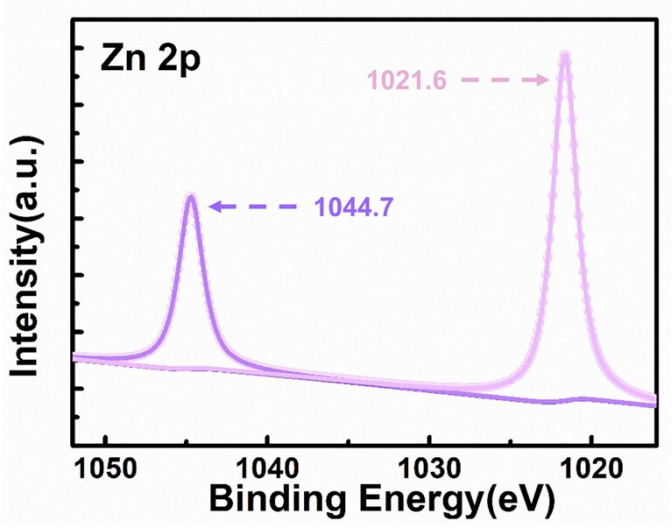

Figure S3. The typical XPS data of Zn 2p, where the peaks detected at 1021.6 eV and 1044.7 eV represents the Zn $2p_{3/2}$ and $2p_{1/2}$, respectively.

S4. The work mechanism of ZnO- based memristor.

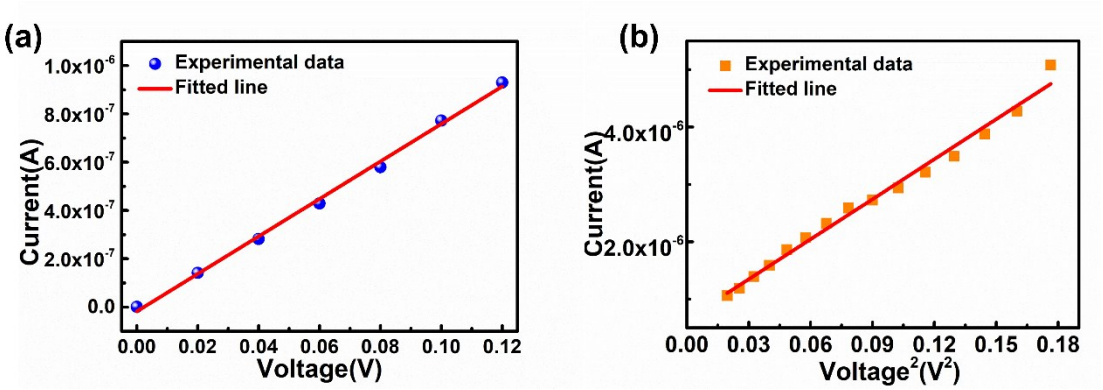

Figure S4. The fitting curves of the device under positive voltage sweep. The fitting curves could be divided to three regions. (a) The Ohmic conduction region. The curve could be fitted well with linear Ohm's law model in this region of 0- 0.12 V, which could be attributed to the effect of intrinsic carrier in film at low voltage.[1] (b) The space-charge- limited current (SCLC) region. In the voltage sweeping range of 0.14- 0.42 V, the replotted curve of I- V^2 suggests the mechanism of SCLC obeying the Child law in the high voltage region of HRS.[2]

S5. The ultralow operating voltages collected from 20 different devices.

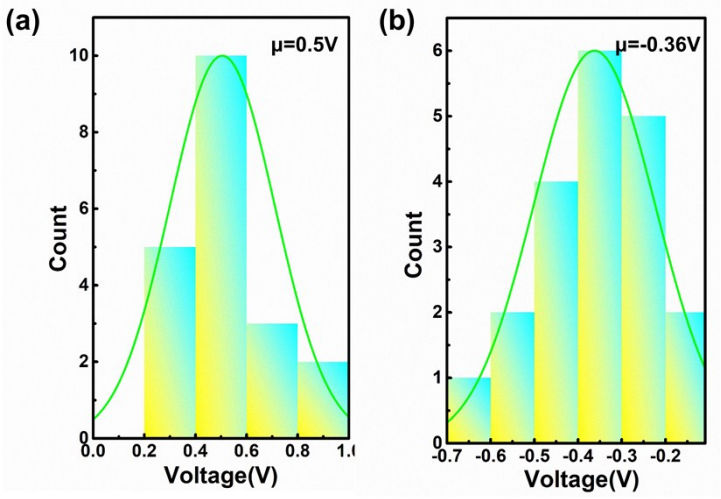

Figure S5. The ultralow positive and negative switching voltages of ZnO- based memristors. (a) The statistical result of set voltages obtained from 20 different ZnO-based devices, where the mean values (μ) is 0.5V. (b) The ultralow μ of reset voltage is -0.36V, which is collected from 20 random devices. These results indicate the reliable ultralow switching voltages in our memristors.

S6. The conduction mechanism of our flexible memristor.

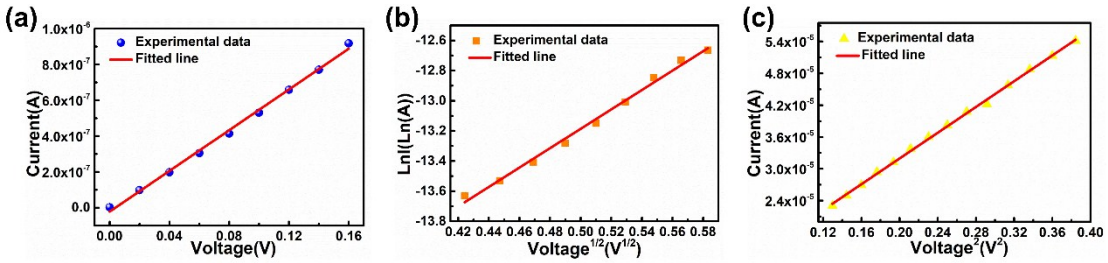

Figure S6. The mechanism fitting results of our memristor under bending state with radius of 10 mm, including three kinds of mechanism model. The fitting result is similar as the device under flat state, including (a) the Ohm's law in the sweeping range of 0- 0.16 V, (b) Schottky model in the region of 0- 0.34 V, and (c) SCLC model in the range of 0.36- 0.62V.

S7. HRS and LRS of device under flat and bending states.

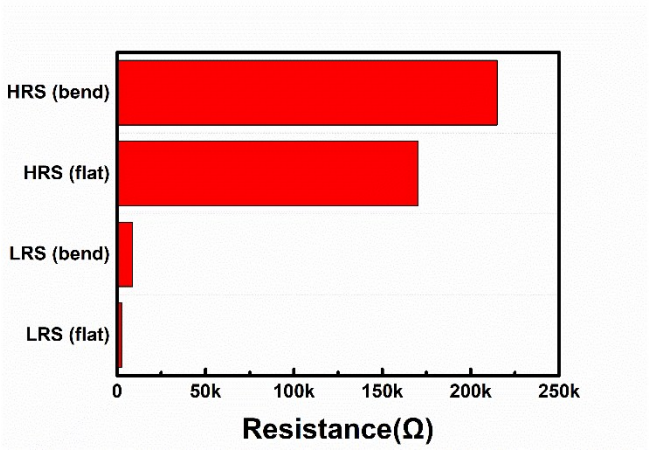

Figure S7. The average values (μ) of resistance of device under flat and bending states. The μ of LRS and HRS under flat state are 2.53 kΩ and 170 kΩ, respectively. Under bending state, the μ of LRS and HRS are 8.69 kΩ and 214.9 kΩ.

S8. The retention time curves of memristor under flat and bending states.

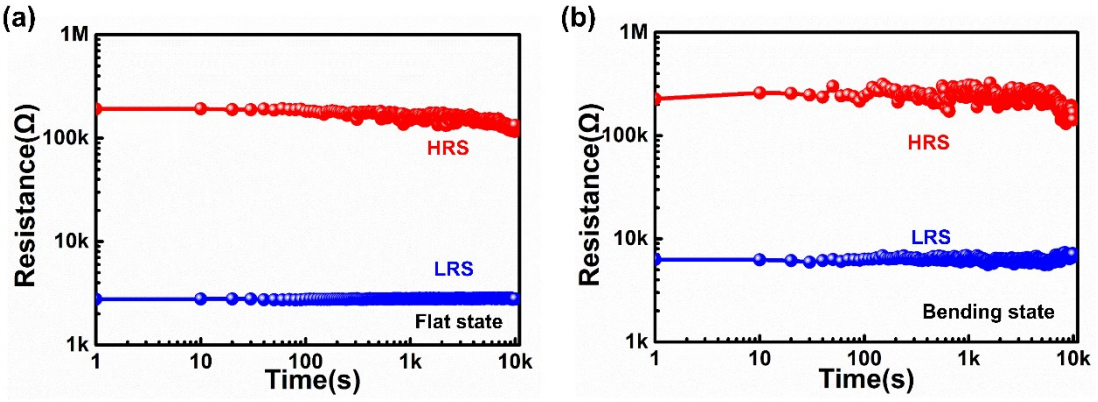

Figure S8. The retention characteristics of device under different testing states. (a) The retention behavior of the ZnO- based device for over 10^4 s with a small bias of 0.1 V. The HRS and LRS show little change after measurement under flat state. (b) The retention curve of device under bending state with radius of 10 mm, where the testing bias is 0.1V. The resistance show little degradation, indicating the reliable characteristic of memristor.

S9. Bending cycle test of flexible memristor.

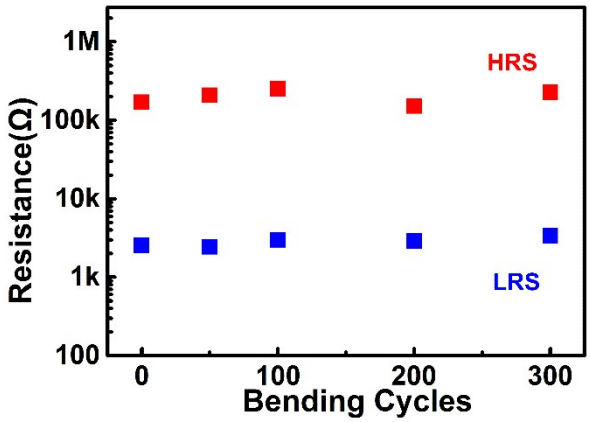

Figure S9. The mechanical flexibility of device under different bending cycles with radius of 10mm. The flexible device exhibits stable HRS and LRS after bending 300 cycles.

S10. The waveforms of pulses used in LTP/LTD measurement.

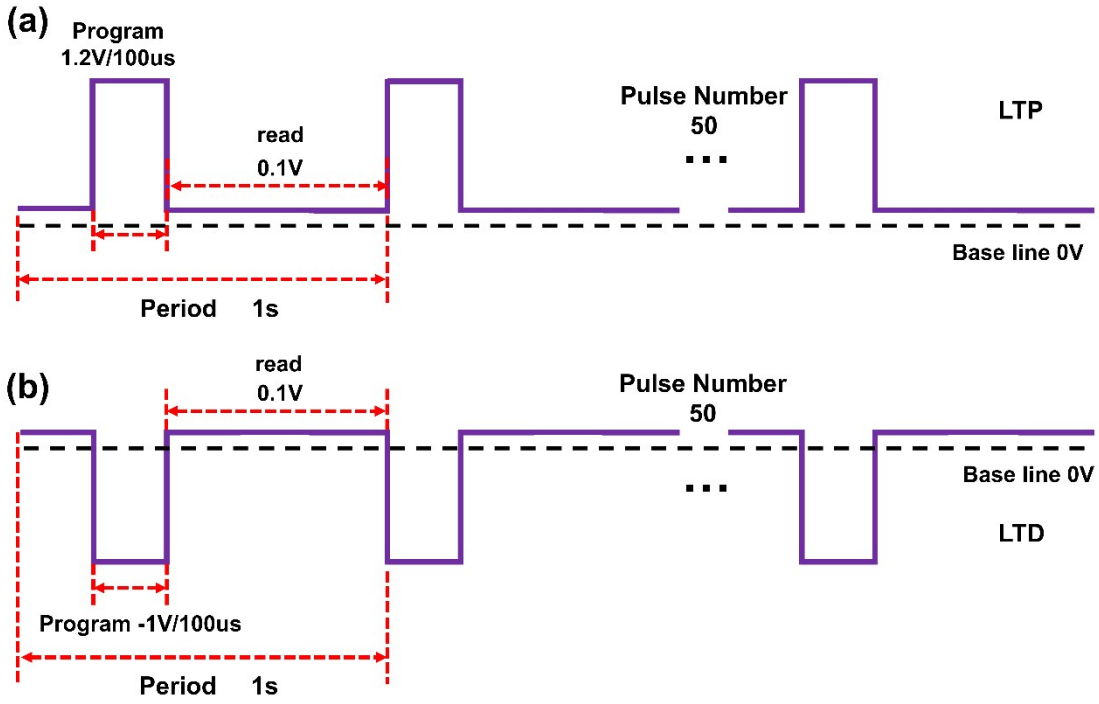

Figure S10. The schematic diagram of waveforms for simulating LTP/LTD behaviors of ZnO- based memristor. (a) The LTP characteristic was emulated by a series of positive pulses (pulse amplitude of 1.2V, width of 100 us, number of 50), where the current is monitored by the small bias of 0.1V. (b) The LTD behavior was simulated by a series of negative pulses (pulse amplitude of -1 V, width of 100 us, number of 50). The bias of 0.1 V was used to monitored the current of device during measurement.

S11. The waveform for long- term retention behavior of device.

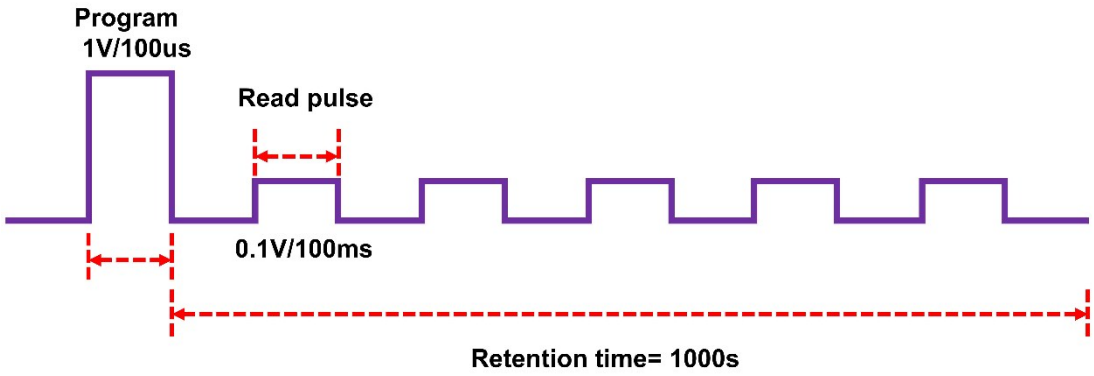

Figure S11. The schematic diagram of waveforms for long- term retention characteristic measurement. The waveforms consist of two kinds of pulses, including the first pulse (pulse amplitude of 1V, width of 100 us, number of 1) for inducing the EPSC behavior of memristor and the rest pulses (pulse amplitude of 0.1V, width of 100 ms) for monitoring the current of memristor over 1000s.

S12. The waveform for PPF behavior of device.

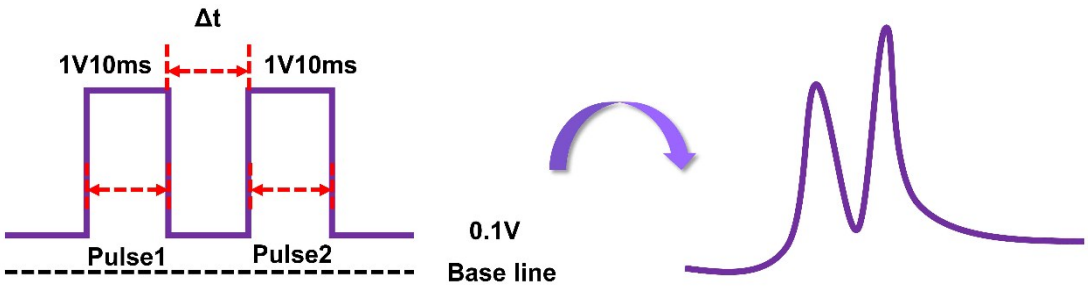

Figure S12. The schematic diagram of waveforms for PPF behavior and the response of post-synaptic current. The waveform consists of a pair of pulses (pulse amplitude of 1V, width of 10 ms, number of 2), where the interval time could be changed for obtaining different PPF index. The post-synaptic current is monitored during all measurement process to simulate the PPF behavior in biology.

Table S1. Comparison of electrical characteristics of several memristors.

Device Architectures	Process Temperature(℃)	Set/Reset Voltage(V)	Uniformity Index	Synaptic Behavior	Flexible	Array Learning	Ref
Ni/h-BN/Au	1050	0.8/-0.7	-	×	×	×	3
rGO/$Ti_3C_2T_x$-PVP/Au	1000	0.9/-1.8	-	×	×	×	4
Ni/Ti/$MoTe_2$/Al_2O_3/Au/Ti	250	2.9/-1.75	-	×	×	×	5
Pt/Ti/SiO_x/Pt/Ti	200	4V/10	-	×	√	×	6
Au/Ti/MoS_2/Ti/Au	170	20/-20	-	√	×	×	7
ITO/ZnO/ Al2O3/TaN	130	1.2/-1.8	35%/40%	√	√	×	8
ITO/BCPO/Al	120	3.2/-3.8	-	√	×	×	9
Au/$MAPbI_3$/Au	100	0.96/-0.55	-	×	×	×	10
Pt/TiO_x/TaO_x/Pt	90	1/-2	-	×	×	×	11
ITO/collagen/Mg	60	2/-3	-	√	√	×	12
Au/Ti/G/h-BN/G/Au	25	3.5V/-1	-	×	×	×	13
ITO/ZnO/TaN	25	0.48/-0.39	5%/10%	√	√	√	This work

Reference

1. Y. Wu, Y. Wei, Y. Huang, F. Cao, D. Yu, X. Li and H. Zeng, *Nano Research*, 2017, **10**, 1584-1594.
2. Y. Wang, Z. Lv, Q. Liao, H. Shan, J. Chen, Y. Zhou, L. Zhou, X. Chen, V. A. L. Roy, Z. Wang, Z. Xu, Y.-J. Zeng and S.-T. Han, *Adv. Mater.*, 2018, **30**, 1800327.
3. X. Wu, R. Ge, P.-A. Chen, H. Chou, Z. Zhang, Y. Zhang, S. Banerjee, M.-H. Chiang, J. C. Lee and D. Akinwande, *Adv. Mater.*, 2019, **31**, 1806790.
4. C. Gu, H.-W. Mao, W.-Q. Tao, Z. Zhou, X.-J. Wang, P. Tan, S. Cheng, W. Huang, L.-B. Sun, X.-Q. Liu and J.-Q. Liu, *ACS Applied Materials & Interfaces*, 2019, **11**, 38061-38067.
5. F. Zhang, H. Zhang, S. Krylyuk, C. A. Milligan, Y. Zhu, D. Y. Zemlyanov, L. A. Bendersky, B. P. Burton, A. V. Davydov and J. Appenzeller, *Nature Materials*, 2019, **18**, 55-61.
6. J. Yoon, Y. Ji, S.-K. Lee, J. Hyon and J. M. Tour, *Advanced Electronic Materials*, 2018, **4**, 1700665.
7. V. K. Sangwan, H.-S. Lee, H. Bergeron, I. Balla, M. E. Beck, K.-S. Chen and M. C. Hersam, *Nature*, 2018, **554**, 500-504.
8. D. Wang, Y. Dai, J. Xu, L. Chen, Q. Sun, P. Zhou, P. Wang, S. Ding and D. W. Zhang, *IEEE Electron Device Lett.*, 2016, **37**, 878-881.
9. J.-Y. Mao, L. Zhou, Y. Ren, J.-Q. Yang, C.-L. Chang, H.-C. Lin, H.-H. Chou, S.-R. Zhang, Y. Zhou and S.-T. Han, *Journal of Materials Chemistry C*, 2019, **7**, 1491-1501.
10. K. Kang, H. Ahn, Y. Song, W. Lee, J. Kim, Y. Kim, D. Yoo and T. Lee, *Adv. Mater.*, 2019, **31**, 1804841.
11. S. Srivastava, J. P. Thomas and K. T. Leung, *Nanoscale*, 2019, **11**, 18159-18168.
12. N. Raeis-Hosseini, Y. Park and J.-S. Lee, *Adv. Funct. Mater.*, 2018, **28**, 1800553.
13. K. Zhu, X. Liang, B. Yuan, M. A. Villena, C. Wen, T. Wang, S. Chen, F. Hui, Y. Shi and M. Lanza, *ACS Applied Materials & Interfaces*, 2019, **11**, 37999-38005.